International Journal of Heat and Mass Transfer 52 (2009) 3084–3090

Contents lists available at ScienceDirect

International Journal of Heat and Mass Transfer

journal homepage: www.elsevier.com/locate/ijhmt

The effects of PE additive on the performance of polystyrene vacuum insulation panels

P.C. Tseng, H.S. Chu *

Department of Mechanical Engineering, National Chiao Tung University, Hsinchu 30049, Taiwan, ROC

ARTICLE INFO

Article history:
Received 21 January 2008
Received in revised form 29 January 2009
Accepted 29 January 2009
Available online 21 March 2009

Keywords:
Broken cell ratio
PS foam insulation
Solid volume fraction

ABSTRACT

The effects of adding polyethylene (PE) in polystyrene (PS) foaming material on the cell structure and the heat transfer of vacuum insulation panels (VIPs) are examined in this study. Several parameters are proposed to describe the foam structure, namely, the broken cell ratio, the average cell size and the solid volume fraction. Adding 2% PE was effective in altering the cell structure and reducing the heat transfer, while adding 5% PE did not improve the performance further. The lowest thermal conductivity found in this study is 4.4 mW m^{-1} K^{-1}, which is among the best published performances of VIP.

1. Introduction

Vacuum insulation panel (VIP) features extremely low thermal conductivity and is suitable for numerous energy conservation applications, such as refrigerator insulation. It is constituted of porous material enclosed in evacuated non-permeable package that is normally made of metal foil envelope. Evacuating the package to a vacuum effectively eliminates the heat transfer by gas convection and conduction. Combining the vacuum with the low thermal conductivity of the porous material, which acts as the VIP's structural support, can greatly reduce overall heat transfer. Commercially available VIPs have currently reached an effective thermal conductivity that is two to six times lower than ordinary foam insulation. The porous cells in the materials must be largely open, that is, broken and connected forming a network so that all the gases can be effectively evacuated. Further reduction in the heat transfer relies on the balance between solid conductive and radiative heat transfer, as we have proposed in an earlier study [1]. Nevertheless, controlling the material structures to obtain optimum performance VIPs is currently still a challenge.

Many previous studies have attempted to determine the heat transfer of solid conduction [2–5], gaseous conduction [5] and thermal radiation [6–18] in porous medium. Most of the studies assumed all closed-cell or all open-cell structures in their analyses. Our earlier work [1] has attempted to characterize the geometrical parameters in VIPs with cell structures in-between all closed-cell and all open-cell, which means that part of the cells are closed and contain gases. It was found that broken cell ratio and cell size have been the deciding factors in reducing thermal transfer. The present study examines the possibility of increasing broken cell ratio by adding polyethylene (PE) into polystyrene in manufacturing the porous materials of VIP. Polyethylene has a higher solidification temperature and becomes hardened when the temperature is still above the melting point of polystyrene. Solidified PE particles could exert shear forces on surrounding molten PS to augment the breaking of closed cells during their expansion in the foaming process. Furthermore, the possibility of modulating cell sizes through PE additives is also examined in detail. Small cell size implies greater solid conduction routes, while large cell size leads to enhanced radiation transport. It is believed there is an optimal cell size that can render the lowest total heat transfer [1]. Adding PE provides a possibility of modulating the cell size and reducing the total heat transfer.

A total of 42 samples with different PE contents, namely, 0 wt%, 2 wt% and 5 wt%, are fabricated in this study. Their heat transfer rates are measured and analyzed. The results will be helpful in manufacturing VIP with improved performance.

2. Experiments

2.1. Sample fabrication

The samples were prepared by the following procedure. A mixture of polystyrene, polyethylene, carbon black, and calcium stearate were put into a batch die of 400 mm diameter and subjected to a 40-ton press. After mixing with the molten mixture, foaming was performed by introducing CO_2 and R-134a into the die to form

* Corresponding author. Tel.: +886 3 571 2121x55115; fax: +886 3 572 7930.
E-mail address: hschu@cc.nctu.edu.tw (H.S. Chu).

0017-9310/$ - see front matter © 2009 Elsevier Ltd. All rights reserved.
doi:10.1016/j.ijheatmasstransfer.2009.01.033

Nomenclature

d_c	cell size, μm
e_b	total emissive power of a blackbody, W m^{-2}
$e_{\lambda b}$	spectral emissive power, W m^{-2} μm^{-1} sr^{-1}
f_s	solid volume fraction, V_s/V_t
f_{s+g}	volume fraction of combined solid and gas
i_λ	spectral intensity of radiant energy
$i_\lambda(0)$	spectral intensity of incident radiation
$i_\lambda(s)$	spectral radiation intensity of a path length s
k_{s+g}	the equivalent thermal conductivity of combined solid and gas
k_r	the thermal radiation conductivity
k_t	the equivalent total thermal conductivity
m	the weight of the sample
q_{s+g}	the heat flux of combined solid and gas
q_r	radiation heat flux
q_t	total heat flux
T	the absolute temperature of the surface, K
V_b	the broken cell volume
V_s	the volume of solid
V_{s+g}	the volume of combined solid and gas in the unbroken cell
V_t	the apparent volume (total volume)
V_{tb}	the volume of all the cells
V_{ub}	the volume of gas in the unbroken cell

Greek symbols

ρ_f	apparent density or foam density, kg m^{-3}
ρ_s	the density of the solid, 991.96 kg m^{-3}
ρ_{s+g}	the density of the combined solid and gas in the unbroken cells, kg m^{-3}
σ	Stefan–Boltzmann constant, 5.67×10^{-8} W m^{-2} K^{-4}
σ_e	Rosseland mean extinction coefficient, Eq. (3)
$\sigma_{e\lambda}$	spectral extinction coefficient, Eq. (4)
τ_λ	spectral transmittance, Eq. (5)

a supercritical fluid. The high pressure gas in the die was released after 6 h, forming a plain board measuring 250 mm long × 250 mm wide × 6–26 mm thick. After about an hour of heating, the material was enclosed by a metal foil envelope, which was sealed after the enclosed air was evacuated to 10^{-4} torr. Experiments were designed to vary the cell geometry of the samples by modulating die temperature and gas pressure. Heaters controlled the die temperature, and maintained a fixed temperature ranging from 398 K to 408 K with a stability of ±0.5 °C throughout the process. Fig. 1 shows the dual pressure control system that was able to separately control the pressure and the amount of CO_2 and R-134a. During the forming process, the gas pressure normally ranged between 2500 psi and 3300 psi. In Fig. 1, the booster pressurizes mixture gas into two pressure tanks. One tank steadily supplies the super critical fluid to liquid tank by the pressure regulator, the other one is as the spare tank. Fig. 2a–c show typical SEM pictures of material samples with 0 wt%, 2 wt% and 5 wt% PE, respectively. The structure typically consists of struts, cell membranes, broken cells and unbroken cells. The average cell size of each sample was calculated by a method in accordance with ASTM standard D 3576-77, using a SEM picture of the sample. The average cell size is 119 μm in Fig. 2a for PE0L4, 211 μm in Fig. 2b for PE2L1, and 262 μm in Fig. 2c for PE5L3.

2.2. Measurements and data reduction

The following method measured radiation's contribution to thermal conductivity. The dimensionless optical thickness of a PS sample is evaluated by multiplying is geometrical thickness from its mean extinction coefficient [19]. For considering optically thick condition, the value has to be far greater than 1. The minimum optical thickness of all the samples in this study is 45, thereby prevailing an optically thick medium that can be treated as a diffusion process. The radiant transfer is simply [20],

$$q_r = -k_r \nabla T = -((16\sigma T_m^3)/(3\sigma_e))\nabla T \quad (1)$$

where the equivalent thermal conductivity is defined as

$$k_r = -(16\sigma T_m^3)/(3\sigma_e) \quad (2)$$

where T_m is the arithmetic mean of the boundary temperatures. The Rosseland mean extinction coefficient (σ_e) is defined as

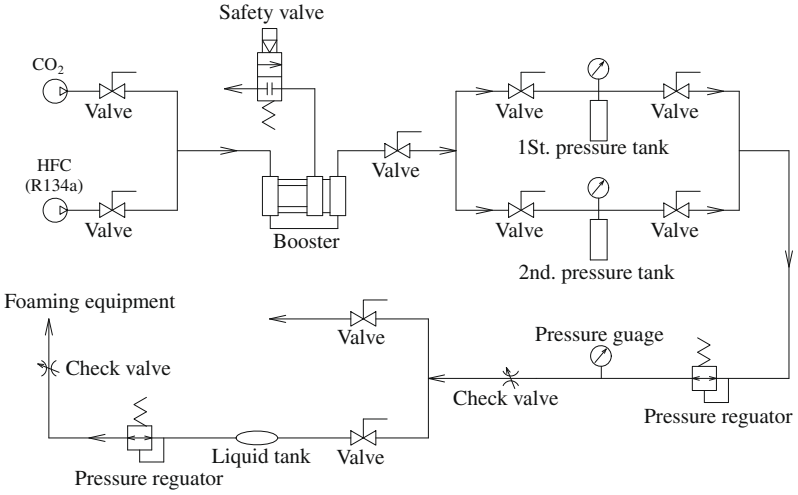

Fig. 1. The schematic process of dual pressure control system for modulating the forming pressure [1].

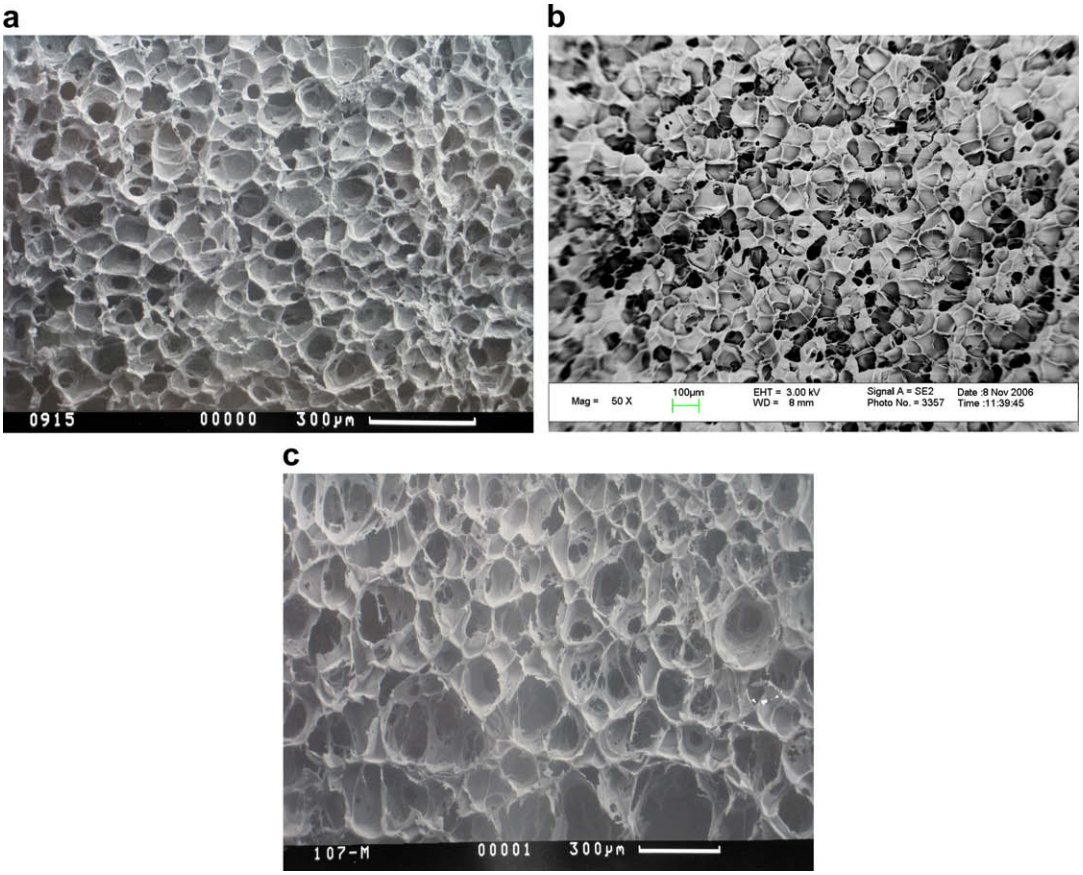

Fig. 2. (a) SEM of sample PE0L4 for PS core material without PE additive [1]. (b) SEM of sample PE2L1 for PS core material with 2% PE additive. (c) SEM of sample PE5L3 for PS core material with 5% PE additive.

$$\frac{1}{\sigma_e} = \int_0^\infty \frac{1}{\sigma_{e\lambda}} \frac{\partial e_{\lambda b}}{\partial e_b} d\lambda \tag{3}$$

where $e_{\lambda b}$ is the spectral emissive power, and e_b is the total emissive power of a blackbody. By neglecting the emission terms and in-scattering terms of a cold homogeneous medium under the influence of a relatively strong but unidirectional beam of radiant energy, the radiation intensity is governed by Beer's law,

$$di_\lambda/ds = -\sigma_{e\lambda} i_\lambda(s) \tag{4}$$

where $\sigma_{e\lambda} = (\sigma_{\alpha\lambda} + \sigma_{s\lambda})$ is the spectral extinction coefficient. The transmittance is defined as

$$\tau_\lambda = i_\lambda(s)/i_\lambda(0) = \exp(-\sigma_{e\lambda} s) \tag{5}$$

The local energy flux (q_t) in VIPs is composed of the transfer by combined gas conduction and solid conduction (q_{s+g}), and by radiation (q_r),

$$q_t = (q_{s+g} + q_r) = -(k_{s+g} + (16\sigma T_m^3)/(3\sigma_e))\nabla T \tag{6}$$

Then, the concept of equivalent thermal conductivity applies,

$$k_t = k_{s+g} + k_r \tag{7}$$

where k_t is the equivalent total thermal conductivity, k_{s+g} is the equivalent thermal conductivity of combined solid and gas, and k_r is the fraction of equivalent thermal conductivity induced by thermal radiation. An EKO model HC-072 conductivity meter was used in this study to measure k_t and keep the temperature difference on both sides of the sample at 0.1 K during the measurements. The equivalent thermal conductivities of all the samples were measured at a hot side temperature of 30 °C and a cold side temperature of 0 °C. The equivalent thermal conductivity is calculated by

$$k_t = (E \cdot L)/(S \cdot \Delta T) \tag{8}$$

where E is the output of the heat-flow meters, L is the thickness of the sample, S is the sensitive of heat-flow meter, and ΔT is the temperature difference between the hot and the cold plate. The equivalent thermal conductivity uncertainty of the data of sample $L3$ is estimated by

$$\begin{aligned}(\delta k/k_t) &= [(k_t/q_t)^2 \delta q_t^2 + (k_t/S)^2 \delta S^2 + (k_t/\Delta T)^2 \delta \Delta T^2]^{0.5}/k_t \\ &= [(6.6/23.34)^2 (0.02)^2 + (6.6/0.00646)^2 (0.00005)^2 \\ &\quad + (6.6/22.8)^2 (0.1)^2]^{0.5}/6.6 \\ &= (0.05896/6.6) = 0.0089\end{aligned} \tag{9}$$

Thus, conductivity measurement uncertainty was controlled to within 0.89%, as estimated by the method of Wu et al. [12].

This study uses a Perkin-Elmer Spectrum 2000 Fourier Transform Infrared Spectrometer to measure the spectral transmittance of each sample. A thinly sliced foam specimen was subjected to normal incident irradiation in the wavelength range of 2.5–25 μm for the measurement. The moisture and volatile organic gas contents of specimens were first removed by an oven. The spectral extinction coefficient ($\sigma_{e\lambda}$) is calculated by Eq. (5) with the measured transmittance. By substituting $\sigma_{e\lambda}$ into Eq. (3), the term σ_e is then calculated. k_r is subsequently obtained by Eq. (2). With the knowledge of k_r and k_t, k_{s+g} can be inferred from Eq. (7). Note that k_r and k_{s+g} reveal the contribution by radiation and combined solid and gas, respectively. To further distinguish the contribution by solid and by gas, this study employs a broken cell

ratio, ϕ, representing the ratio of broken cell volume to the total cell volume

$$\phi = \frac{V_b}{V_{tb}} = \frac{V_t - (m/\rho_{s+g})}{V_t - (m/\rho_s)} = \frac{(m/\rho_f) - (m/\rho_{s+g})}{(m/\rho_f) - (m/\rho_s)} = \frac{\rho_s}{\rho_{s+g}} \frac{(\rho_{s+g} - \rho_f)}{(\rho_s - \rho_f)} \quad (10)$$

where V_b or the broken cell volume is the vacuum volume inside the VIP (which actually contains air in extremely low pressure), V_{tb} is the volume of all the cells, V_t is the apparent volume (total volume), m is the weight of the sample, $\rho_{s+g} = m/V_{s+g} = m/(V_{ub} + V_s)$ is the density of the combined solid and gas in the unbroken cells, V_{s+g} is the volume of combined solid and gas in the unbroken cell, V_{ub} is the volume of gas in the unbroken cell, and V_s is the volume of solid. The apparent density, or foam density, $\rho_f = m/V_t$, was measured using the ASTM D-1622 method. Note that this approach disregards the weight of the extremely low-pressure gas in the vacuum. Subtracting the broken cell volume from the total volume produces V_{s+g}. The former was measured by an AccuPyc 1330 Pycnometer with an accuracy of 0.03%. The term ρ_s is the density of the solid, taken as the density of the raw polystyrene, which is 991.96 kg m^{-3}.

The solid volume fraction, f_s, is the ratio of solid volume to the total volume and is readily obtained by dividing the foam density of the sample by the polystyrene density.

$$f_s = V_s/V_t = 1 - [(1 - f_{s+g})/\phi] \quad (11)$$

3. Results and discussion

Table 1 summarizes the measurement results of the samples without PE additive. The samples fall into two distinct groups with different solid volume fraction. The first group, referred to as PE0L, has a lower solid volume fraction, and includes PE0L1 to PE0L6 with $0.0413 < f_s < 0.0494$. The second group, referred to as PE0H, has a higher solid volume fraction and includes PE0H1 to PE0H8 with $0.065 < f_s < 0.0706$. Similar results of samples with 2.0 wt% and 5.0 wt% PE additive are also listed in Table 1, respectively. Similar to the samples without PE additive in Table 1, each PE additive contains two distinct groups with different solid volume fraction. The groups with higher solid volume fraction are designated as PE2H and PE5H, and the groups with lower solid volume fraction are designated as PE2L and PE5L, for the 2% and 5% PE samples, respectively. Note that all solid volume fractions in the 42 investigated samples are extremely low (less than 0.07), indicating a good foaming process. Nevertheless, the distinction between high and low solid volume fractions in each table is sharp and allows us to investigate the effects of solid volume fraction.

Figs. 3 and 4 show examples of spectral transmittance and spectral extinction coefficient, respectively. Note that the spectra do not reveal any CO_2 absorption, which could occur at 2.7 μm,

Table 1
The characteristics of PS core material with 0%PE, 2%PE and 5%PE in vacuum insulation panel.

No. of samples	ρ_f (kg m^{-3})	ρ_{f+g} (kg m^{-3})	f_s	ϕ	d_c (μm)	σ_e (m^{-1})	k_r (mW m^{-1} K^{-1})	k_{s+g} (mW m^{-1} K^{-1})	k_t (mW m^{-1} K^{-1})
PE0L1	49	704	0.0494	0.9787	143	5397	1.336	5.46	6.8
PE0L2	47	623	0.0474	0.9705	138	5999.2	1.202	5.50	6.7
PE0L3	44	565	0.0444	0.9649	130	6653.1	1.084	5.52	6.6
PE0L4	43	486	0.0433	0.9528	119	9645.9	0.749	5.75	6.5
PE0L5	42	388	0.0423	0.9312	100	13818.1	0.519	6.48	7.0
PE0L6	41	347	0.0413	0.9198	85	21887.6	0.327	7.37	7.7
PE0H1	70	812	0.0706	0.9832	374	5231.8	1.368	6.73	8.1
PE0H2	69	782	0.0696	0.9799	369	5999.2	1.187	6.71	7.9
PE0H3	68	736	0.0686	0.9744	330	6291.2	1.132	6.67	7.8
PE0H4	65	709	0.0655	0.9720	318	6750.3	1.059	6.64	7.7
PE0H5	64	692	0.0645	0.9701	305	7677.3	0.928	6.67	7.6
PE0H6	63	626	0.0635	0.9604	250	10758.7	0.664	7.24	7.9
PE0H7	62	561	0.0625	0.9488	175	15149.4	0.472	7.83	8.3
PE0H8	61	450	0.0615	0.9211	110	20886.1	0.341	8.66	9.0
PE2L1	30	675	0.0302	0.9854	211	11535.9	0.713	3.89	4.6
PE2L2	29	627	0.0292	0.9825	196	12862.9	0.639	3.86	4.5
PE2L3	28	560	0.0282	0.9776	175	14643.3	0.561	3.84	4.4
PE2L4	26	502	0.0262	0.9737	152	15842.2	0.518	4.48	5.0
PE2L5	25	448	0.0252	0.9686	140	17153.1	0.479	4.82	5.3
PE2H1	52	761	0.0524	0.9832	252	12825.8	0.640	4.66	5.3
PE2H2	51	732	0.0514	0.9808	238	13729.1	0.598	4.60	5.2
PE2H3	49	695	0.0494	0.9778	212	14920.2	0.552	4.55	5.1
PE2H4	48	668	0.0484	0.9753	191	15482.9	0.531	5.07	5.6
PE2H5	47	637	0.0474	0.9723	177	16655.2	0.495	5.31	5.8
PE5L1	49	762	0.0494	0.9843	264	5488.4	1.497	5.90	7.4
PE5L2	49	695	0.0492	0.9778	263	5545.8	1.484	5.72	7.2
PE5L3	48	579	0.0476	0.9637	262	6081.8	1.352	5.85	7.2
PE5L4	47	540	0.0465	0.9584	245	6959.4	1.181	5.92	7.1
PE5L5	46	473	0.0464	0.9466	240	8643.4	0.953	6.05	7
PE5L6	46	452	0.0454	0.9419	239	8664.4	0.949	6.05	7
PE5L7	46	382	0.0451	0.9224	220	9669.6	0.849	5.95	6.8
PE5L8	45	334	0.0444	0.9064	180	15161.5	0.540	6.56	7.1
PE5L9	44	319	0.0436	0.9021	145	16771.1	0.488	7.11	7.6
PE5H1	65	706	0.0655	0.9716	302	6420	1.279	6.62	7.9
PE5H2	64	655	0.0649	0.9645	296	6750.7	1.214	6.49	7.7
PE5H3	64	523	0.0647	0.9592	276	6891.5	1.189	6.51	7.7
PE5H4	63	509	0.0638	0.9357	251	9658.9	0.850	6.45	7.3
PE5H5	63	476	0.0635	0.9265	226	11612.5	0.707	6.49	7.2
PE5H6	62	460	0.0626	0.9229	241	12452.4	0.658	6.44	7.1
PE5H7	61	440	0.0617	0.9178	217	13162.3	0.624	6.68	7.3
PE5H8	61	431	0.0616	0.9147	197	14666.1	0.599	6.9	7.5
PE5H9	60	393	0.0604	0.9019	140	18567.8	0.441	7.56	8.0

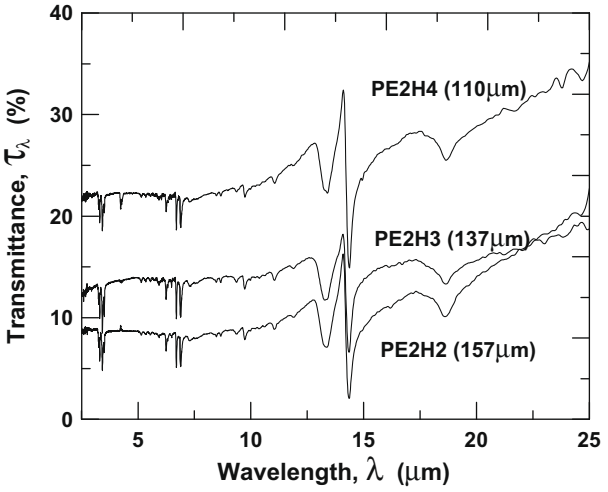

Fig. 3. Spectral transmittance varied with wavelength on PE2H samples.

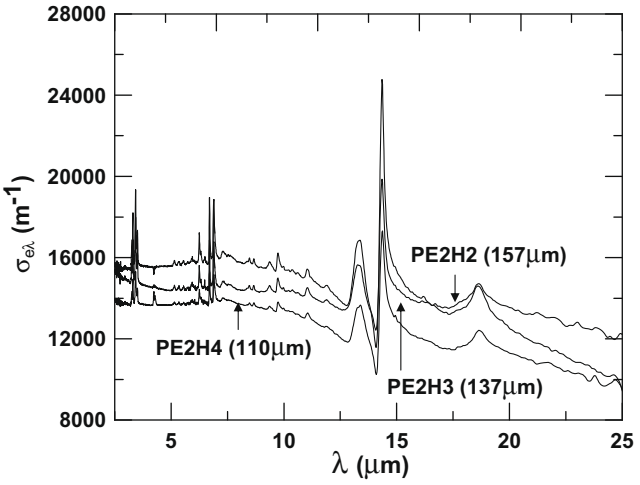

Fig. 4. Spectral extinction coefficient varied with wavelength on PE2H samples.

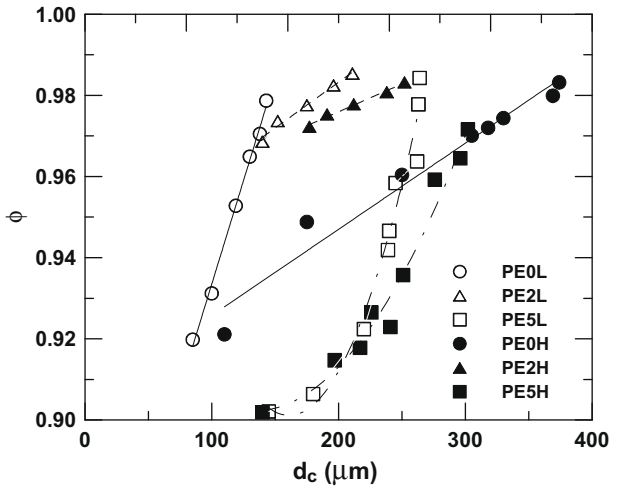

Fig. 5. Relationship between cell sizes and broken cell ratio on various PE additives with high and low solid volume fraction.

4.3 μm, 9.4 μm, 10.4 μm, and 15 μm, or H_2O absorption, which could occur at 2.7 μm and 6.3 μm. This indicates that the amount of CO_2 and H_2O trapped in the unbroken cells is insignificant in terms of influencing radiation heat transfer. This is reasonable since most of the cells in the samples are broken and evacuated.

Fig. 5 plots the broken cell ratio versus the cell size. Each group shows an almost linear dependence of cell size on open cell ratio. Higher solid volume fraction is typically associated with larger cell size for a given PE additive weight percentage. The trend can be explained by the fact that a higher solid volume allows the cells to expand further before breaking. In the meantime, in order to obtain a higher broken cell ratio, more of the unbroken cells must be expanded further until they are broken, which also increases the average cell size. Different slopes of the relationship between broken cell ratio and cell size for different PE additive weight percentages in Fig. 5 are attributed to the effects of PE on the strength of cell membranes. These effects are also responsible for the larger cell sizes of PE2 and PE5 when compared to PE0. PE0H is an exception because its solid volume fraction is too high, which leads to large cell size as explained earlier. PE's high melting temperature makes them more likely to solidify than PS during the cooling process in foaming and create membrane shear stress when the cells are growing, which helps to raise the broken cell ratio. If the PE additive is too much, however, the cell membrane strength could be augmented too much and the cells would grow larger without becoming broken. It will become evident in the following discussion that 2% PE is appropriate in terms of balancing cell size and broken cell ratio, while 5% PE leads to larger cell size and lower broken cell ratio. To summarize, cell size is influenced by three parameters, the broken cell ratio, the solid volume fraction and the PE additive. Among which, the PE additive is the easiest one to control and is an effective way to modify cell morphology.

Figs. 6 and 7 plot the Rosseland mean extinction coefficient against variations in cell size and broken cell ratio, respectively. The extinction coefficient in VIP consists of two parts, the absorption part, σ_α, and the scattering part, σ_s, that is, $\sigma_e = \sigma_\alpha + \sigma_s$. The former represents the absorption effect of solid material and depends largely on the solid volume fraction. The latter is affected by the morphology of the porous foam structure, which is characterized by the average cell size and the broken cell ratio. Smaller cell size implies a shorter mean free path and a larger scattering coefficient for thermal radiation. The mean extinction coefficient therefore increases as the cell size decreases, as evident in Fig. 6. For a given PE additive percentage, Fig. 7, the group with higher solid volume fraction exhibits only a slight increase in extinction coefficient compared with the lower solid volume fraction group,

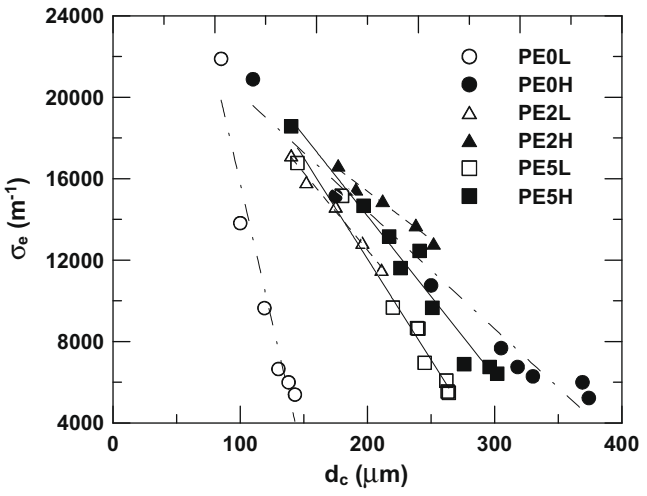

Fig. 6. Rosseland mean extinction coefficient varied with cell sizes with/without PE additives on high and low solid volume fraction.

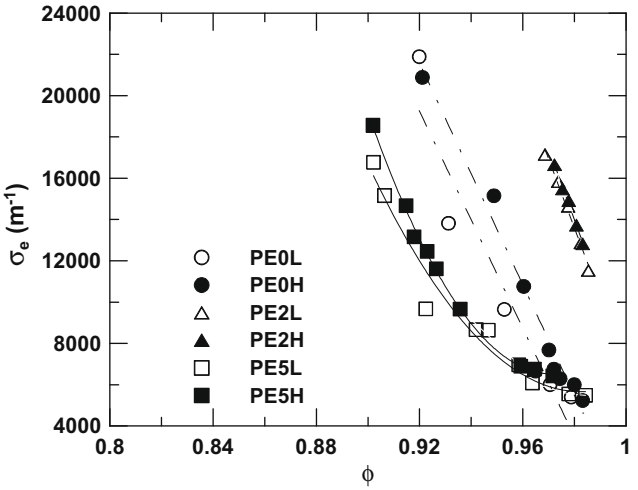

Fig. 7. Rosseland mean extinction coefficient varied with broken cell ratio with/without PE additives on high and low solid volume fraction.

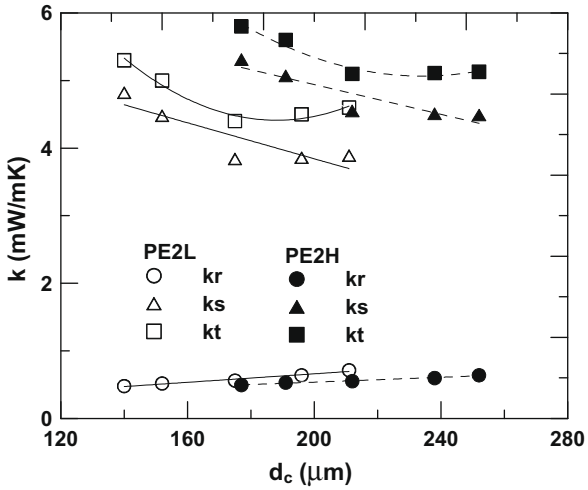

Fig. 9. The relation between equivalent thermal conductivity and cell sizes for PS core material with 2% PE additive.

although the average solid volume fractions of the two groups differ significantly. This can be explained by the fact that the solid volume fraction of all the samples are so small that the extinction is dominated by scattering and the solid absorption contribution is relatively insignificant. Extinction coefficients generally decrease as the broken cell ratio increases, as shown in Fig. 7, due to reduced scattering by closed cell membrane. Although radiation extinction is a complex process influenced by cell morphology, the broken cell ratio proposed in this study is a suitable parameter to correlate the extinction coefficient for a given PE additive percentage. Adding 2% PE is effective in increasing the extinction coefficient, due mainly to the alteration of cell morphology. Increasing the PE additive to 5% does not increase the extinction further. On the contrary, the extinction at the same broken cell ratio drops to a lower amount than the case without PE additive. This can be explained partly by the fact that the cell size has grown too large in 5% PE samples. The trend in Figs. 6 and 7 should be examined carefully, as the cell size, the solid volume fraction and the broken cell ratio all appear to influence the extinction coefficient. Nevertheless, the apparent higher extinction coefficient for higher solid volume fraction shown in Fig. 6 can be explained by the lower broken cell ratio associated with higher solid volume fraction, as evident in Fig. 5.

Fig. 8 shows the equivalent thermal conductivities of samples without PE additive, including the total thermal conductivity, k_t, the thermal conductivity by solid/gas conduction, k_{s+g}, and the thermal conductivity by radiation, k_r. The total thermal conductivity of the lower solid volume fraction group, PE0L is generally lower than that of the higher solid volume fraction group, PE0H. This difference is mainly caused by a change in solid/gas conduction, which accounts for more than 80% of the heat transfer in the samples. Also, solid/gas conduction increases as the cell sizes decrease, which is associated with lower broken cell ratio and creates more conduction transport routes in the material. On the other hand, radiation decreases as the cell size decreases. Note that the decrease in radiation (increase in extinction coefficient) is attributable to the change in broken cell ratio, as explained earlier. Consequently, there is a best cell size (best broken cell ratio), which leads to the lowest total thermal conductivity after combining k_{s+g} and k_r for each group of samples. In Fig. 8, the lowest total thermal conductivity is around 6.5 mW m^{-1} K^{-1}, which occurs in the PE0L group at a broken cell ratio of approximately 0.95 corresponding to a cell size of about 100 μm. Figs. 9 and 10 shows the equivalent thermal conductivities of PE2 and PE5 groups, respectively, with trends similar to that in Fig. 7. The best cell size of

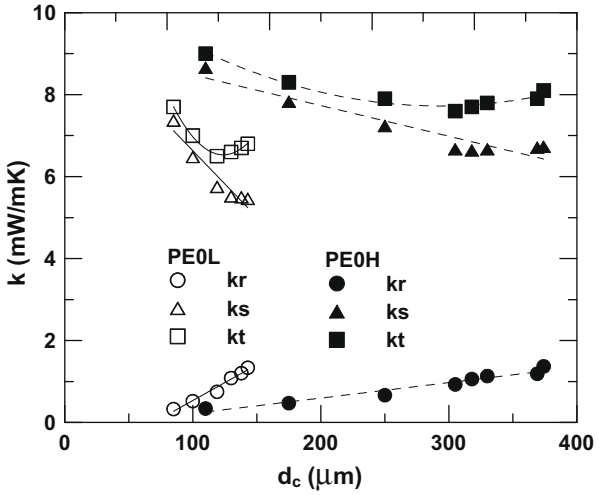

Fig. 8. The relation between equivalent thermal conductivity and cell sizes for PS core material without PE additive.

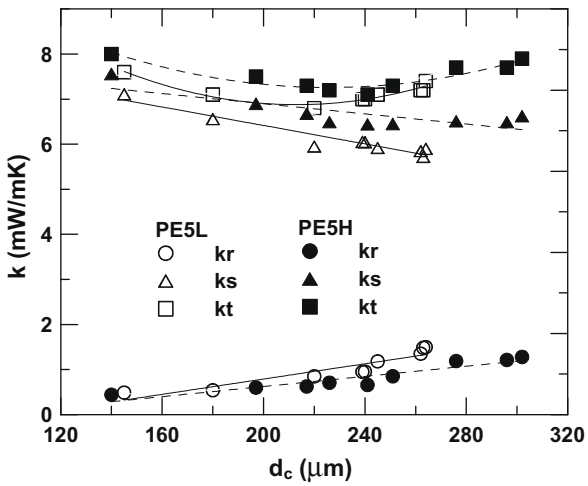

Fig. 10. The relation between equivalent thermal conductivity and cell sizes for PS core material with 5% PE additive.

the 2% PE group, Fig. 9, falls at around 170 μm, resulting in a total thermal conductivity of 4.4 mW m^{-1} K^{-1}, which is the lowest in all the samples investigated in this study. Increasing the PE additive to 5% does not reduce the total thermal conductivity further. Both solid/gas conduction and radiation are enhanced in the 5% PE groups when compared to 2% PE group. The enhanced radiation could be explained by the alteration in cell morphology and the enhanced solid/gas conduction is explained by the lower broken cell ratios of the 5% PE groups, as discussed earlier.

4. Conclusions

This study analyzes heat transfer in practical VIP, that is, VIP with a broken cell ratio higher than 90%. The structure of these non-black-body VIP foams consists of struts, closed cells and open cell residue membranes. PE additive is used as a way to alter the foam structure and the heat transfer. Two parameters, namely, the broken cell ratio and the average cell size, are proposed to characterize the structure. The experimental samples are further grouped based on their solid volume fraction to reveal the influence of the solid material on heat transfer. Some conclusions derived from the experimental findings may help improve VIP performance, as summarized below.

1. Under a specific solid volume fraction, a best cell size (best broken cell ratio) leads to the lowest total thermal conductivity.
2. Radiation heat transfer, as manifested by the mean extinction coefficient, is influenced predominantly by broken cell ratio. The effects of solid volume fraction upon radiation are relatively insignificant in the samples investigated in this study. PE2 samples have smaller cell size and therefore higher extinction than PE5 samples.
3. An appropriate amount of PE additive has proven to be effective in tuning the cell structure and improving the VIP performance. The best PE content among the three additive percentages investigated in this study was 2%.
4. Solid volume could affect the absorption coefficient in radiation transfer, but the effects are not obvious because the solid volume fraction is extremely low in this study, and the extinction coefficient is dominated by scattering. However, the solid volume fraction has a crucial effect on solid conduction, which is the dominant heat transfer mechanism in VIP. A rule of thumb to improve VIP permeance can be derived from the findings in this study. Firstly, the solid volume fraction must be kept low to diminish the solid conduction. Secondly, the cell size and broken cell ratio must be carefully controlled to an optimum value to produce the lowest total thermal conductivity. A high broken cell ratio may cause high radiation transfer, and does not necessarily imply low total thermal conductivity. In contrast to conventional closed-cell foam, where a small cell size reduces the heat transfer of trapped gas, the best cell size in practical VIP with high broken cell ratio ranges from 100 to 300 μm. The lowest thermal conductivity obtained in this study reached 4.4 mW m^{-1} K^{-1}, and was among the best when previously compared to published VIP performance results.

References

[1] P.C. Tseng, H.S. Chu, An experimental study of the heat transfer in PS foam insulation, Heat Mass Transfer 45 (4) (2009) 399–406.
[2] H.S. Chu, A.J. Stretton, C.L. Tien, Radiative heat transfer in ultra-fine powder insulations, Int. J. Heat Mass Transfer 31 (8) (1988) 1627–1634.
[3] A.M. Druma, M.K. Alam, C. Druma, Analysis of thermal conduction in carbon foams, Int. J. Thermal Sci. 43 (2004) 689–695.
[4] V. Giaretto, E. Miraldi, G. Ruscica, Simultaneous estimations of radiative and conductive properties in lightweight insulating materials, High Temp. – High Pressures 27/28 (1995/1996) 191–204.
[5] J. Kuhn, H.P. Ebert, M.C. Arduini-Schuster, D. Buttner, J. Fricke, Thermal transport in polystyrene and polyurethane foam insulations, Int. J. Heat Mass Transfer 35 (7) (1992) 1795–1801.
[6] D. Quenard, D. Giraud, Heat transfer in the packing of cellular pellets: microstructure and apparent thermal conductivity, High Temp. – High Pressures 30 (6) (1998) 709–715.
[7] D. Doermann, J.F. Sacadura, Heat transfer in open cell foam insulation, ASME J. Heat Transfer 118 (1996) 88–93.
[8] D. Baillis, M. Arduini-Schuster, J.F. Sacadura, Identification of spectral radiative properties of polyurethane foam from hemispherical and bi-directional transmittance and reflectance measurements, J. Quant. Spectrosc. Radiative Transfer 73 (2002) 297–306.
[9] L.R. Glicksman, M.R. Torpey, The influence of cell size and foam density on the thermal conductivity of foam insulation, Polyurethanes World Congress, Aachen, Germany, 1987, pp. 80–84.
[10] L.R. Glicksman, A.L. Marge, J.D. Moreno, Radiation heat transfer in cellular foam insulation, ASME Paper HTD-203, 1992, pp. 45–53.
[11] K. Kamiuto, Study of Dul'nev's model for the thermal and radiative properties of open-cellular porous materials, JSME Int. J. Ser. B 40 (4) (1997) 577–582.
[12] J.W. Wu, W.F. Sung, H.S. Chu, Thermal conductivity of polyurethane foams, Int. J. Heat Mass Transfer 42 (1999) 2211–2217.
[13] R. Caps, U. Heinemann, J. Fricke, K. Keller, Thermal conductivity of polymide foams, J. Heat Mass Transfer 40 (2) (1997) 269–280.
[14] R. Coquard, D. Baillis, Modeling of heat transfer in low-density EPS foams, ASME J. Heat Transfer 128 (2006) 538–549.
[15] M. Loretz, R. Coquard, D. Baillis, E. Maire, Metallic: radiative properties/comparison between different modes, J. Quant. Spectrosc. Radiative Transfer 109 (2008) 16–27.
[16] C.Y. Zhao, T.J. Lu, H.P. Hodson, Thermal radiation in ultralight metal foams with open cells, Int. J. Heat Mass Transfer 47 (2004) 2927–2939.
[17] C. De Micco, C.M. Aldao, Radiation contribution to the thermal conductivity of plastic foams, J. Polym. Sci. B Polym. 43 (2005) 190–192.
[18] E. Placido, M.C. Arduini-Schuster, J. Kuhn, Thermal properties predictive model for insulating foams, Infrared Phys. Technol. 46 (2005) 219–231.
[19] M.N. özisik, Radiative Transfer and Interactions with Conduction and Convection, John Wiley & Sons, New York, 1973.
[20] R. Siegel, J.R. Howell, Thermal Radiation Heat Transfer, fourth ed., Taylor & Francis, New York, London, 2002.